JETS AND WINDS FROM GAMMA-RAY BURSTS*

Agnieszka Janiuk

Center for Theoretical Physics of the Polish Academy of Sciences
Al. Lotników 32/46, 02-668 Warsaw, Poland

Received 30 May 2022, accepted 3 June 2022,
published online 9 September 2022

We investigate the properties of short and long gamma-ray burst jets launched from accreting black holes. We run the numerical general relativistic simulations in a magneto-hydrodynamic setup and we study the connection between properties of the jet and the accretion disk as its central engine. Our simulations show that the formation of magnetically arrested disk state is important for the jet launching process. The variability of the jets as measured at their base is intrinsically related to the timescales of magneto-rotational instability in the accretion disk. In addition, magnetically driven winds from the accretion disk influence the jet properties and, in some cases, may lead to its quenching. Finally, in short GRB engines, these winds are sites of r-process nucleosynthesis and contribute to the kilonova signal, observed at longer wavelengths after the prompt GRB emission.

DOI:10.5506/APhysPolBSupp.15.3-A17

1. Introduction

Accreting black holes act as the central engines of various observed astrophysical phenomena such as gamma-ray bursts, quasars, and blazars. The multi-wavelength observations of the accretion systems show different kinds of outflows. The collimated outflows usually referred to as jets are sites of emission of high-energy photons with spectral energy distribution peaking in the gamma-ray band and characterized by rapid variability (see [1] for a review on GRBs, and [2] for a discussion of blazar samples observed by Swift). Strong gravity acts on the accreting material in such systems due to the presence of a compact central object. The central object can either be a neutron star, a stellar mass black hole (~ 3 to $20 M_{\odot}$, in the case of black hole X-ray binaries or gamma-ray bursts), or a super-massive black hole ($\sim 10^5$ to $10^{10} M_{\odot}$, in the case of active galactic nuclei). Relativistic

* Presented at the 28$^{\text{th}}$ Cracow Epiphany Conference on *Recent Advances in Astroparticle Physics*, Cracow, Poland, 10–14 January, 2022.

jets are believed to be powered by the Blandford–Znajek mechanism [3], which can extract the rotational energy of the black hole. This mechanism requires a poloidal magnetic field built up in the vicinity of the black hole due to continuous accretion.

Jets in Active Galaxies and GRBs are powered by accretion of magnetized plasma. Charged particles gyrate around the magnetic field lines and produce synchrotron radiation. The strength of magnetic field depends on various environmental factors in the vicinity central engine. The turbulence in accretion flows can result in the magneto-rotational instability (MRI) [4], which transports angular momentum outwards in the disk and effectively drives accretion.

On the other hand, if the plasma is threaded by a large-scale magnetic field, the inflow of matter to the central engine can be affected in a different way. This can occur due to a variety of reasons, such as dragging the external magnetic field with the flow, or the field inheritance from the past history of the progenitor or host. In such cases, the central object accumulates a large amount of poloidal flux as the accretion proceeds. The accumulated flux cannot fall into the black hole, only matter can fall in. This flux cannot escape either, due to the inward pressure of accretion. The structure is then regulated by the interchange instabilities. Thus, the infalling matter is arrested due to the action of magnetic fields and further accretion is only possible in shorter episodes. For achieving the MAD state, the simulation must enforce a substantial accumulation of magnetic flux over time. Such a state is often termed as magnetically arrested disk (or MAD) [5, 6].

The class of short gamma-ray bursts originates from binary neutron star mergers. This theoretical prediction has been proven for the first time by the gravitational wave detection from the source GW 170817 [7], which preceded a short gamma-ray burst observed 1.7 seconds later on. Radioactivities from dynamical ejecta after the first neutron disruption may power an electromagnetic signal [8–10]. The subsequent accretion can provide bluer emission, if it is not absorbed by precedent ejecta [11]. In this case, a day-timescale emission comes at optical wavelengths from lanthanide-free components of the ejecta, and is followed by week-long emission with a spectral peak in the near-infrared (NIR). This two-component model fits well with observations of the kilonova, detected in coincidence with the GRB-GW 170817 source.

2. Numerical modelling

2.1. Code

In order to study the formation and evolution of jets, we compute the structure and evolution of a black hole accretion torus by evolving the general relativistic magnetohydrodynamic (GRMHD) equations in time. We use

the HARM (High Accuracy Relativistic Magnetohydrodynamics) code [12] which is a conservative and shock- capturing scheme. The numerical scheme advances the conserved quantities from one time step to the next by solving a set of non-linear equations, in each time step. We follow the flow evolution by solving numerically the continuity, energy-momentum conservation, and induction equations in the GRMHD scheme

$$\nabla_\mu(\rho u^\mu) = 0\,, \qquad \nabla_\mu(T^{\mu\nu}) = 0\,, \qquad \nabla_\mu(u^\nu b^\mu - u^\mu b^\nu) = 0\,, \tag{1}$$

$$T^{\mu\nu} = T^{\mu\nu}_{\rm gas} + T^{\mu\nu}_{\rm EM}\,, \tag{2}$$

$$T^{\mu\nu}_{\rm gas} = \rho h u^\mu u^\nu + p g^{\mu\nu} = (\rho + u + p) u^\mu u^\nu + p g^{\mu\nu}, \tag{3}$$

$$T^{\mu\nu}_{\rm EM} = b^2 u^\mu u^\nu + \tfrac{1}{2} b^2 g^{\mu\nu} - b^\mu b^\nu\,, \qquad b^\mu = u^*_\nu F^{\mu\nu}\,. \tag{4}$$

Here, the stress-energy tensor is comprised of the gas and electromagnetic terms, u^μ is the four-velocity of the gas, u is the internal energy, ρ is the density, p is the pressure, and b^μ is the magnetic four vector. F is the Faraday tensor and in a force-free approximation, we have $E_\nu = u^\nu F^{\mu\nu} = 0$. The unit convention is adopted such that $G = c = M = 1$ and thus the black hole mass will scale the simulations (*e.g.* gravitational radius $r_{\rm g} = GM_{\rm BH}/c^2$ or time $t_{\rm g} = GM_{\rm BH}/c^3$).

2.2. Simulation setup

Our initial condition for the simulation assumes a pressure equilibrium torus as described by Fishbone and Moncrief [13]. In this solution, the angular momentum along the radius of the disk is a constant. In our model, we use a polytropic equation of state, $p_{\rm g} = K\rho^\gamma$, where $p_{\rm g}$ is the gas pressure, ρ is the density, and K is the constant specific entropy. We use the value of $4/3$ for the polytropic index γ.

We study a sequence of models with various Kerr parameters, $a = 0.9$, and $a = 0.6$. We run simulations in 3D with a resolution $288 \times 256 \times 256$ in the r, θ, and ϕ directions, respectively. The outer edge of the grid is located at $R_{\rm out} = 10^5$ gravitational radii, and inner radius is located at $R_{\rm in} = 0.87 \times (1. + \sqrt{(1. - a^2)})$, below the black hole horizon. The numerical code works in the Kerr–Schild coordinates, which enables the matter to smoothly accrete under the horizon, without being affected by singularities. The numerical grid is non-uniform, and a progressively sparser grid starts at $R_{\rm br} = 400$, with $x^{(1)}_i = x^{(1)}_{i-1} + 1/C \times \delta x$, where $\delta x = x^{(1)}_i - (\log(R_{\rm br} - R_0))^4$. We use $C = 1$ to limit the hyper-exponentiation.

The initial size of the disk is prescribed using the inner edge of disk, and the radius of pressure maximum and they have the values $r_{\rm in} = 6$ and $r_{\rm max} = 13.5 r_{\rm g}$, respectively. The relative difference of the two radii determines also the dimension of the torus and the specific angular momentum value, which in the Fishbone–Moncrief solution is constant over radius. For our parameters, it is equal to $l_{\rm spec} = 4.397$.

The initial torus is embedded in a poloidal magnetic field, prescribed with the vector potential of

$$A_\varphi = \left(\frac{\bar{\rho}}{\rho_{\max}} - \rho_0 \right) r^5 \,, \tag{5}$$

where $\bar{\rho}$ is the density in the torus (averaged over 2 neighbouring cells), $\rho_{\max}$ is the density maximum, and we use $\rho_0 = 0.2$. The factor of r^5 ensures that higher magnetic flux will be brought onto the black hole horizon from larger distances, as the evolution proceeds. Other spatial components of the initial vector potential are zero, $A_r = A_\theta = 0$, hence the magnetic field vector will have only B_r and B_θ components. The vector potential is related to the Faraday tensor, $F_{\mu\nu} = \partial_\mu A_\mu - \partial_\nu A_\mu$, and hence we get the magnetic field 'four-vectors' with $b^\mu = -{}^*F^{\mu\nu} u_\nu$. It is related to the normal observers magnetic field vector, as $B^\mu = \alpha {}^*F^{\mu t}$, where $\alpha = 1/g_{tt}$ is the lapse (note that there is no time component of B^μ).

We use the plasma β-parameter, which is defined as the ratio of the gas-to-magnetic pressure, $\beta = p_{\rm gas}/p_{\rm mag}$, to scale the initial magnetic field. Here, $p_{\rm gas} = (\gamma - 1) u_{\max}$ and $p_{\rm mag} = b^2_{\max}/2$, where $u_{\max}$ is the internal energy of the gas at the radius of maximum pressure. We normalize β to a chosen value at the radius of maximum gas pressure, $r_{\max}$ inside the torus. Initial β is a free parameter of our model. We examine several models with different minimal initial β of the plasma: the tested values were 30, 50, and 100.

The code works in dimensionless units $c = G = M = 1$. For the purpose of these computations, we keep the scaling, and the black hole mass M does not change during the simulation. In physical scales, the GRB engines are modelled with mass of the black hole $M_{\rm BH}$, the torus mass, which gives the scaling of distance, time, density, and accretion rate of the infalling matter. For GRB engines, we adopt the density scaling that is constrained by the mass of torus enclosed in the simulation volume so that $D_{\rm unit} = M_{\rm unit}/L^3_{\rm unit} = 3.45 \times 10^{11}$ g cm^{-3}, where $M_{\rm unit}$ scales the total mass of the torus, and $L_{\rm unit} \equiv r_{\rm g}$ is scaled by the black hole mass. The magnetic flux is then normalized with $\Phi_{\rm unit} = \sqrt{4\pi D_{\rm unit} c^2} L^2_{\rm unit} = 1.042 \times 10^{18}$ Gs cm^2.

3. Results

The accretion flow under the influence of the initially poloidal magnetic field is subject to the turbulence and the matter starts falling inward to the central object due to transport of angular momentum outwards by the MRI. The accreting plasma brings in more poloidal magnetic flux to the black hole. This flux gets accumulated and after some time it hinders with the accretion and the disk gets arrested.

The structure of the flow in the evolved state is shown in Fig. 1. We present polar and equatorial slices taken at the mod time of the simulation of a GRB central engine. Parameters of this model are $a = 0.3$ and $\beta = 100$. We show the cuts of a small region of $10r_{\rm g}$ from the black hole (bottom panels), and the cuts showing large regions, up to $100r_{\rm g}$ (top panels). As shown in these maps, the magnetically arrested flow appeared in this simulation, and forced the accretion to proceed via the azimuthally distributed 'fingers', surrounding the black hole and entering its horizon. The zoomed equatorial plots show that the magnetic field lines are pulled into the black hole within the low-density regions, while the high-density fingers are pushing out the

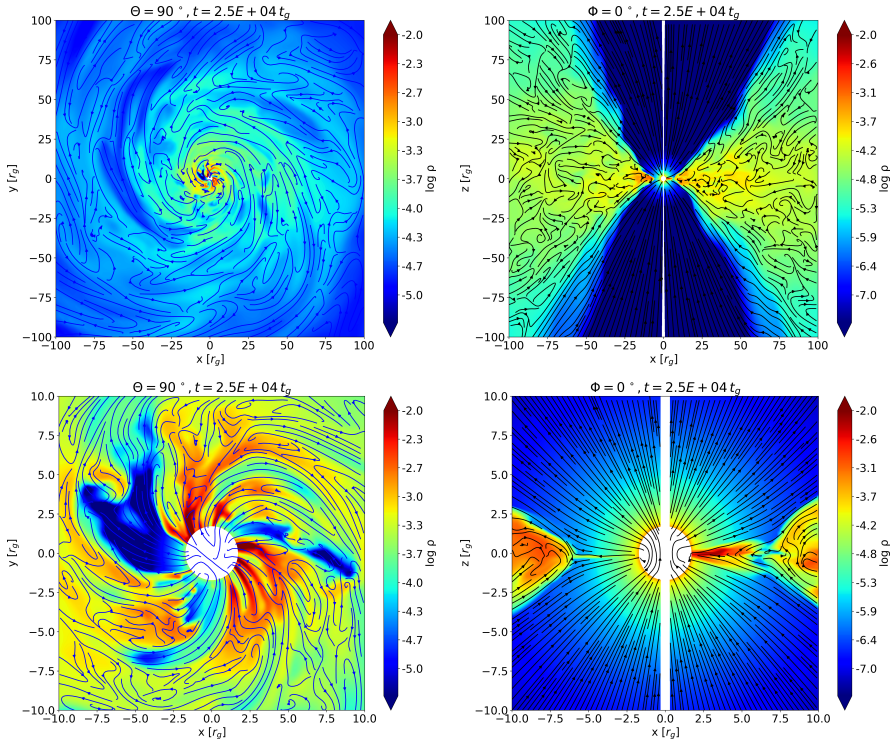

Fig. 1. (Colour on-line) Maps of the density isocontours in the equatorial plane XY (left column) and in the polar plane XZ (right column). Top panels are scaled to a distance of 100 $r_{\rm g}$, while bottom panels are zoom-in and show the region within 10 $r_{\rm g}$. The model represents a central engine composed of a spinning black hole and magnetically arrested disk. Its parameters are gas-to-magnetic pressure ratio $\beta = 100$ and black hole spin $a = 0.3$. The color maps are in logarithmic scale and are taken at the intermediate time of the simulation, at $t = 25,000t_{\rm g}$ (in geometric units, *i.e.*, equivalent to ~ 0.3 seconds for $M_{\rm BH} = 3M_{\odot}$). Streamlines show the magnetic 3-vector configuration.

magnetic fields. Thus, the magnetic tension can locally push the gas out and suppress the accretion rate, while in the denser regions, the matter prevents the flux from entering the horizon. We also note that when the jet forms, there appear hot luminous regions near the black hole rotation axis, which have a very low baryon density and a vertically oriented magnetic field. These polar regions represent bi-polar jets, with the luminosity that depends on the black hole spin.

In Fig. 2, we show the time-dependence of the so-called MAD-ness parameter, *i.e.* the ratio of the mass and magnetic flux through the black hole horizon. This dimensionless flux is given by the relations

$$\dot{m}_{\rm BH} = -\int \rho u^r \sqrt{-g}\, {\rm d}\theta\, {\rm d}\phi\,, \tag{6}$$

$$\Phi_{\rm BH} = 0.5 \int |B^r| \sqrt{-g}\, {\rm d}\theta\, {\rm d}\phi\,, \tag{7}$$

and

$$\phi_{\rm BH} = \frac{\Phi_{\rm BH}}{\sqrt{\dot{m}_{\rm BH}}}\,. \tag{8}$$

As shown in Fig. 2, the magnetic flux that has been dragged to the black hole vicinity, grows high enough to capture the accretion flow. Hence, the ratio of the mass and magnetic fluxes remains constant and larger than $\phi_{\rm BH} \sim 10$ for most of the simulation, after the initial condition is relaxed.

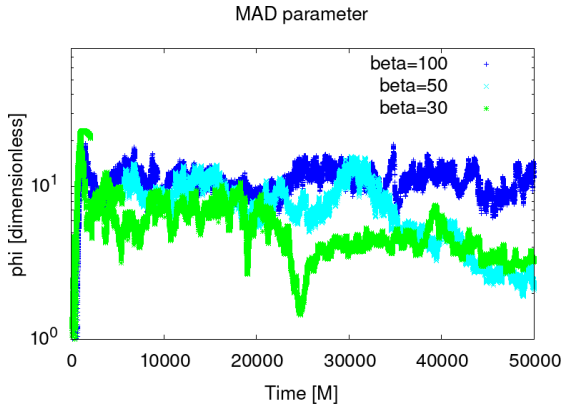

Fig. 2. (Colour on-line) Time dependence of the so-called MAD-ness parameter, $\phi_{\rm BH}$, given by Eq. (8). Blue (black) lines denote the models with initial gas-to-magnetic pressure ratio $\beta = 100$, cyan (light grey) lines present results for $\beta = 50$, and green (grey) lines denote $\beta = 30$. Black hole spin parameter in all models is $a = 0.9$.

We investigate the evolution of the jet by studying the jet energetics parameter

$$\mu = -T^{\rm r}_t / \rho u^{\rm r} \tag{9}$$

which is the total plasma energy flux normalized to the mass flux. Here, $T^{\rm r}_t$ is the energy component of the energy-momentum tensor, ρ is the gas density, and $u^{\rm r}$ is the radial velocity. Figure 3 shows the structure of the jet depicted as a distribution of its energetics parameter μ. It is taken at a specific time snapshot in the mid-time of the simulation, *i.e.* $t = 25,000\, t_{\rm g}$. We plot the jet structure along two different ϕ slices and show that the structure is not axisymmetric. It can be observed from these plots that the jet emission is not continuous but intermittent. Note that such a jet emission is observed along with the MAD state where the accretion proceeds in short episodes rather than in a continuous flow of matter to the central object.

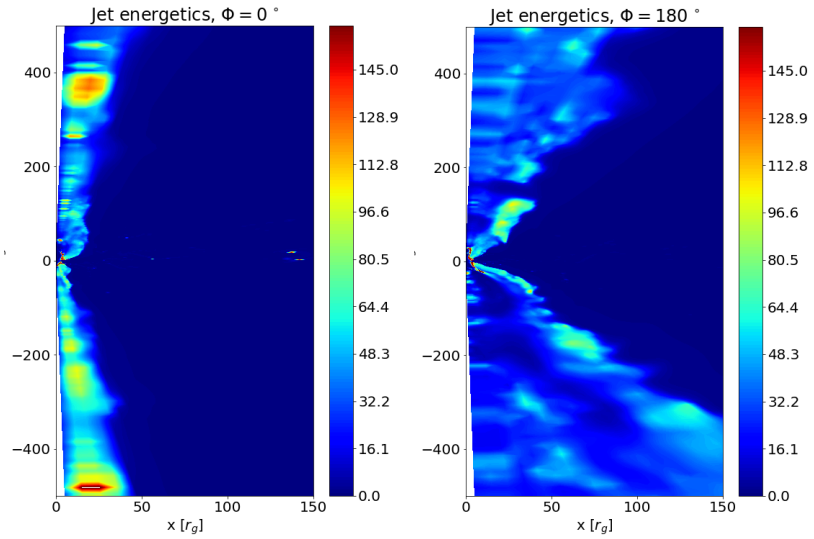

Fig. 3. Profiles of jet energetics, defined by μ-parameter, see Eq. (9), for the GRB model with high spin, $a = 0.9$ and $\beta = 50$. The maps show profiles taken at two opposite azimuthal angles, $\Phi = 0$ and $\Phi = \pi$. Snapshots are taken at time $t = 2.5 \times 10^4 t_{\rm g}$.

The power of the jet is computed using an estimate of the Blandford–Znajek process, where the rotating black hole is surrounded by a force-free, magnetized plasma. We use the formula given by [14]

$$P_{\rm BZ} = -\int\limits_{r=r_{\rm h}} \left(b^2 u^{\rm r} u_t - b^{\rm r} b_t\right) {\rm d}A\,, \tag{10}$$

so that we integrate the radial part of electromagnetic flux over the surface of black hole horizon. In the above formula, we neglect the matter component, assuming a force-free approximation. For a steady, uniform outflow, this expression gives the radial Poynting energy flux measured by a stationary observer at a large distance from the black hole. We notice that the BZ power is positive only if the energy can be extracted to the remote jets from the black hole, so only the flux with a negative sign (*i.e.* entering the horizon) will contribute to it. Otherwise, there is no energy extraction from the black hole via the BZ process.

In Fig. 4, we show the GRB jet power as a function of time. We present the simulations with black hole spin $a = 0.9$ and we show the power (in code units) for various disk magnetisations. We find that strong powerful jets are emitted in most models with high black hole spin, and that the jet power depends on the initial disk magnetisation. The initial power of the jet is small, then, after a transient peak due to fast accretion, it aims to reach an equilibrium value and, finally, it drops by 2–3 orders of magnitude by the end of the runs. For the smallest initial β-parameter, the jet is weak, and it gets quenched at the mid-time of simulation (its BZ power drops to zero). The same occurs with the jet emitted in $\beta = 50$ case, albeit only at the end of the run. This behaviour is correlated with the decrease of the dimensionless magnetic flux, $\phi_{\rm BH}$ (*cf.* Fig. 2), which means that the MAD state is not sustained in these models, apart from the case of $\beta = 100$. Strikingly, a large initial gas pressure brings more magnetic flux to the black hole and helps in sustaining a powerful, steady jet.

On the other hand, larger magnetic pressure seems to have an impact on the disk winds. In the currently presented 3D simulation, we do not include a quantitative measure of the disk wind (we used tracer particles in our 2D simulations, see the next section). However, we aim to qualitatively estimate the power transferred to the equatorial winds, and check whether it depends on the model magnetisation. In Fig. 5, we plot the mass outflow rate through the outer boundary as a function of time for several simulations of the GRB central engine. As shown in the figure, the mass outflow is negligible at the beginning of the simulation, when the initial condition of the pressure equilibrium torus is being relaxed. However, after some 0.3 seconds (which corresponds to about $20000\,t_{\rm g}$), the outflow rate value is larger and some mass is left from the system via winds. At the end of the simulation, the outflow rate is again below $10^{-3} M_{\odot}\,{\rm s}^{-1}$. We notice that both higher black hole spin and higher magnetic pressure result in more powerful outflows, and the maximum amplitude of the mass loss rate during the simulation scales with these parameters. This is qualitatively consistent with the findings by [15], where the winds were studied in the context of r-process nucleosynthesis.

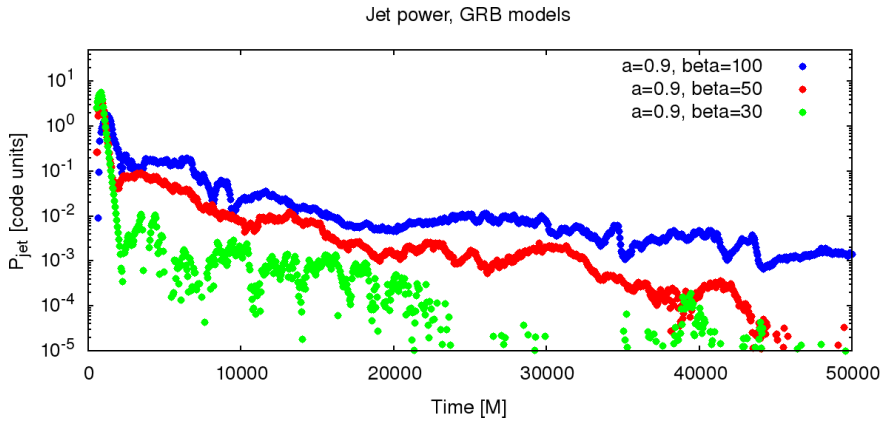

Fig. 4. (Colour on-line) Power of the Blandford–Znajek process, calculated from Eq. (10), as a function of time. We present models of GRB engine with high black hole spin $a = 0.9$. Three colours denote different initial disk β-parameters, shown with blue (top), red (middle), and green (bottom) points for $\beta = 100$, 50, and 30, respectively.

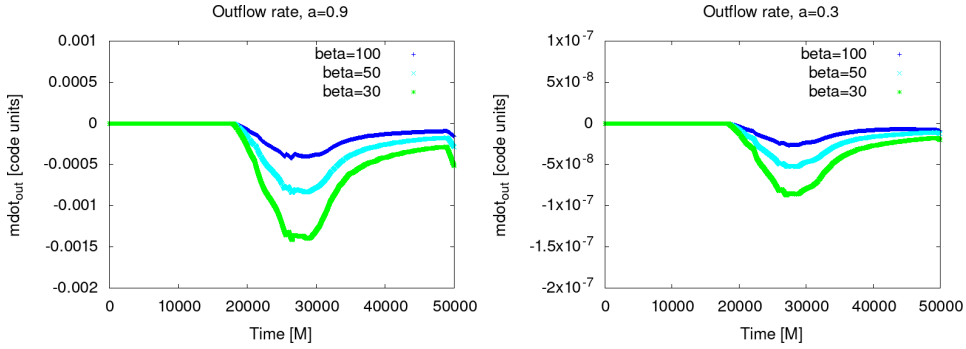

Fig. 5. (Colour on-line) Mass outflow rate though the outer boundary, for GRB models with high and low spin, shown in the left and right panels, for $a = 0.9$ and $a = 0.3$, respectively. Three colors mark different initial gas-to-magnetic pressure ratio, β.

4. Accretion disk winds in short GRBs

To study the evolution of a post-merger disk addressed to the engine of a short GRB, we supplement our computations with a nuclear equation of state (EOS) module, which substitutes the adiabatic EOS used in the MAD disk/jet simulations reported above. The microphysics of the torus formed just after the disruption of a neutron star is determined by the nuclear temperatures and densities, hence using Fermi gas EOS and account

for partial degeneracy of nucleons and electrons or positrons, seems more physical. What is more important, in this way we can follow the process of neutronisation of plasma, as quantified by the so-called electron fraction

$$Y_e = \frac{n_{e^-} - n_{e^+}}{n_b}\,, \tag{11}$$

where in the nominator, the number density of electrons and positrons, is balanced by protons, due to the charge neutrality. The number densities of all species are given by their Fermi–Dirac distributions over their chemical potentials and relativity parameters, $\beta_i = kT_i/(m_i c^2)$. The total pressure is contributed by free nucleons, pairs, radiation, alpha particles, and trapped neutrinos (see details in [15]). The neutrinos which are created in weak interactions, and also the electron–positron pair annihilation, nucleon bremsstrahlung, and plasmon decay, provide a cooling mechanism for the accretion disk. In the current model, we use a simplified description of the total neutrino cooling rate given by the two-stream approximation [16], which includes the scattering and absorptive optical depths for neutrinos of the three flavours. The neutrino emissivity distribution image taken at an evolved state of the torus is presented in Fig. 6. As can be seen in the map, the accreting torus has a very high neutrino luminosity, but here neutrinos are partially trapped. A moderately high neutrino luminosity can be observed from the wind, where the neutrino–antineutrino pairs can contribute to the heating of the plasma. A detailed calculation with the neutrino transfer is needed to quantify this effect.

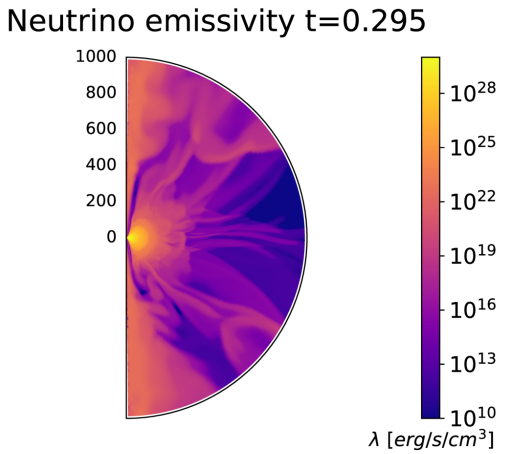

Fig. 6. Neutrino emissivity distribution in the evolved short GRB engine model. Model parameters are gas-to-magnetic pressure ratio $\beta = 10$ and black hole spin $a = 0.6$.

We show that the accretion disk launches fast wind outflows, $v \sim$(0.11–0.23) c, with a broad range of electron fraction $Y_e \sim$ (0.1–0.4). The mass loss via unbound outflows is between 2% and 17% of the initial disk mass [15]. The details are sensitive to engine parameters: BH spin and magnetisation of the disk and more magnetized disk produce faster outflows, as shown in Fig. 7. The plot shows velocity of the wind averaged over about 1000–2000 tracer particles, which were recorded as leaving the outer boundary of our central engine computational domain, and the extrapolated to later times. The results account for heating feedback, calculated from the nuclear reaction network.

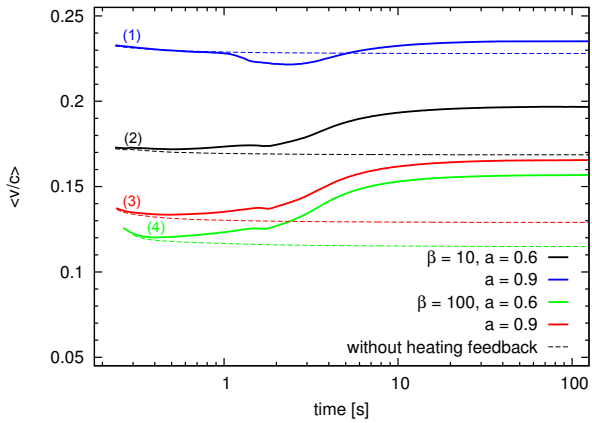

Fig. 7. (Colour on-line) Time dependence of wind velocity in short GRB models. Black (2) and blue (1) lines denote the models with initial gas-to-magnetic pressure ratio $\beta = 10$, green (4) and red (3) lines present results for $\beta = 100$. Black hole spin parameter was $a = 0.6$ and $a = 0.9$, respectively.

To follow the nucleosynthesis process, we used code SkyNet, which provides a nuclear reaction network [17]. The software contains a large database of over a thousand isotopes and computes nuclear reaction rates for a given density, temperature, and electron fraction value. It is capable to trace the nucleosynthesis in the rapid neutron capture process, including self-heating.

We found that the accretion disk ejecta produce heavy elements up to mass number $A \sim 200$, including platinium and gold isotopes, as shown in Fig. 8. These wind outflows should presumably contribute to the kilonova signal, due to radioactive decay of unstable r-process isotopes, synthesized under the high neutronisation conditions in these ejecta.

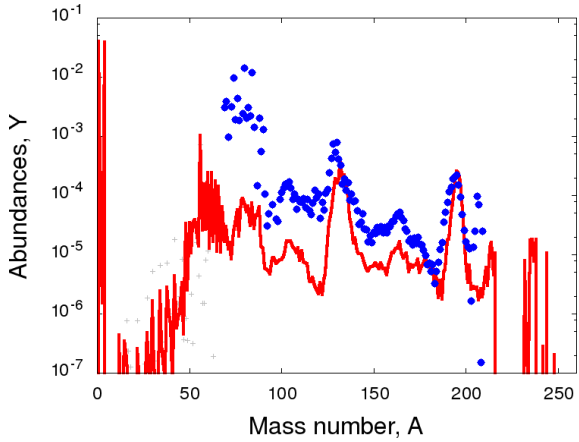

Fig. 8. (Colour on-line) The abundance pattern of the elements synthesized in the accretion disk wind. Blue points denote the solar abundance pattern. Red line represents the average abundance distribution of elements synthesized in the disk wind via r-process. Model initial gas-to-magnetic pressure ratio is $\beta = 10$, and the black hole spin parameter is $a = 0.9$.

5. Conclusions

We study both 2D and fully 3D general relativistic numerical simulations of accretion flows of a magnetically arrested state of accretion disk. We find that they adequately describe engines of gamma-ray bursts. Our 3D simulations adopt an adiabatic equation of state that neglects the microphysics effects and are performed in a dimensionless setup. The variability modelling is based on the fact that the timescales of flares and the time variability of energy injection to the jets are scaled with geometric time, $t_{\rm g} = GM_{\rm BH}c^{-3}$. Therefore, they can be directly compared to the variability of gamma-ray emission in long and short GRBs down to millisecond timescales, and correlated with the burst duration [18]. In the study presented in detail by [19], we explain an observed correlation between the jet Lorentz factor and the minimum variability timescale of GRB, which was observationally motivated by the work of [20].

The variability of prompt emission of GRBs is related to both the variability of the central engine itself, or to the interaction of the jet with the progenitor star envelope in a long GRB case [21]. The engine and jet base variability is driven by magneto-rotational instability, or interchange instabilities in MAD disks, which we cover in the presented simulations. The jet may also interact with the disk winds, which are expected to accompany the short GRB prompt phase. As our results show, such an interaction can occur only for a limited period of time, when the wind mass loss rate

is largest and when the jet can be partially or completely chocked. The unbound outflows, *i.e.* winds, are in principle powered by both neutrinos and magnetically-driven acceleration. Therefore, winds may be more dense and powerful, if the neutrino-driven mechanism supports or substitutes the magnetically-driven wind [22].

The MHD simulations show that rotational instabilities have an imprint on the variability of the jet. The same MHD mechanism drives the disk wind. The role of disk wind is specifically important for the short GRBs, where the central engine of the jet is formed after the NS–NS binary merger. The accretion disk around the newly formed black hole ejects material rich in heavy radioactive isotopes. They are formed in the rapid neutron capture process (r-process). The r-process nucleosynthesis in the accretion disk outflows can provide additional contribution to the kilonova emission, in addition to the pre-merger ejecta launched in the form of tidal tails. Observationally testable results, motivated by the recently discovered electromagnetic counterparts of gravitational wave source GW170817, require two-component modelling.

Finally, we speculate that the jet interactions with wind shape its radiative properties and together with pre-merger dynamical ejecta may explain time-delay between GW and GRB signals. This can be an alternative explanation of the timescales, apart from the commonly adopted lifetime scale of the hypermassive neutron star, which might have formed before the black hole was created.

This work was supported by grant 2019/35/B/ST9/04000 from the National Science Center, Poland (NCN). We used computational resources of the ICM of the University of Warsaw, and the PL-Grid, under grant plggrb5.

REFERENCES

[1] N. Gehrels, E. Ramirez-Ruiz, D.B. Fox, «Gamma-Ray Bursts in the *Swift* Era», *Annu. Rev. Astron. Astrophys.* **47**, 567 (2009).

[2] P. Giommi *et al.*, «X-ray spectra, light curves and SEDs of blazars frequently observed by Swift», *Mon. Not. R. Astron. Soc.* **507**, 5690 (2021).

[3] R.D. Blandford, R.L. Znajek, «Electromagnetic extraction of energy from Kerr black holes», *Mon. Not. R. Astron. Soc.* **179**, 433 (1977).

[4] S.A. Balbus, J.F. Hawley, «A Powerful Local Shear Instability in Weakly Magnetized Disks. I. Linear Analysis», *Astrophys. J.* **376**, 214 (1991).

[5] I.V. Igumenshchev, «Magnetically Arrested Disks and the Origin of Poynting Jets: A Numerical Study», *Astrophys. J.* **677**, 317 (2008).

[6] A. Tchekhovskoy, R. Narayan, J.C. McKinney, «Efficient generation of jets from magnetically arrested accretion on a rapidly spinning black hole», *Mon. Not. R. Astron. Soc.* **418**, L79 (2011).

[7] B.P. Abbott *et al.*, «Gravitational Waves and Gamma-Rays from a Binary Neutron Star Merger: GW170817 and GRB 170817A», *Astrophys. J. Lett.* **848**, L13 (2017).

[8] L.-X. Li, B. Paczyński, «Transient Events from Neutron Star Mergers», *Astrophys. J.* **507**, L59 (1998).

[9] N.R. Tanvir *et al.*, «A 'kilonova' associated with the short-duration γ-ray burst GRB 130603B», *Nature* **500**, 547 (2013).

[10] O. Korobkin, S. Rosswog, A. Arcones, C. Winteler, «On the astrophysical robustness of the neutron star merger r-process», *Mon. Not. R. Astron. Soc.* **426**, 1940 (2012).

[11] D.M. Siegel, B.D. Metzger, «Three-Dimensional General-Relativistic Magnetohydrodynamic Simulations of Remnant Accretion Disks from Neutron Star Mergers: Outflows and r-Process Nucleosynthesis», *Phys. Rev. Lett.* **119**, 231102 (2017).

[12] C.F. Gammie, J.C. McKinney, G. Tóth, «HARM: A Numerical Scheme for General Relativistic Magnetohydrodynamics», *Astrophys. J.* **589**, 444 (2003).

[13] L.G. Fishbone, V. Moncrief, «Relativistic Fluid Disks in Orbit Around Kerr Black Holes», *Astrophys. J.* **207**, 962 (1976).

[14] J.C. McKinney, C.F. Gammie, «A Measurement of the Electromagnetic Luminosity of a Kerr Black Hole», *Astrophys. J.* **611**, 977 (2004).

[15] A. Janiuk, «The r-process Nucleosynthesis in the Outflows from Short GRB Accretion Disks», *Astrophys. J.* **882**, 163 (2019).

[16] T. Di Matteo, R. Perna, R. Narayan, «Neutrino Trapping and Accretion Models for Gamma-Ray Bursts», *Astrophys. J.* **579**, 706 (2002).

[17] J. Lippuner, L.F. Roberts, «SkyNet: A Modular Nuclear Reaction Network Library», *Astrophys. J. Suppl. Ser.* **233**, 18 (2017).

[18] G.A. MacLachlan *et al.*, «Minimum variability time-scales of long and short GRBs», *Mon. Not. R. Astron. Soc.* **432**, 857 (2013).

[19] A. Janiuk, B. James, I. Palit, «Variability of Magnetically Dominated Jets from Accreting Black Holes», *Astrophys. J.* **917**, 102 (2021).

[20] Q. Wu *et al.*, «The extension of variability properties in gamma-ray bursts to blazars», *Mon. Not. R. Astron. Soc.* **455**, L1 (2016).

[21] B.J. Morsony, D. Lazzati, M.C. Begelman, «The Origin and Propagation of Variability in the Outflows of Long-duration Gamma-ray Bursts», *Astrophys. J.* **723**, 267 (2010).

[22] A. Murguia-Berthier *et al.*, «The Fate of the Merger Remnant in GW170817 and Its Imprint on the Jet Structure», *Astrophys. J.* **908**, 152 (2021).